Cell-free reconstitution of HIV-1 innate immune sensing reveals the capsid is a molecular cloak that protects reverse transcripts from cGAS

Authors:

Tiana M. Scott[1], Lydia M. Arnold[1], Jordan A. Powers[1], Delaney A. McCann[1], Devin E. Christensen[2], Wen Zhou[3], Rachel M. Torrez[2], Janet H. Iwasa[2], Philip J. Kranzusch[4,5], Wesley I. Sundquist[2], Jarrod S. Johnson[1,*]

Affiliations:

[1]Division of Microbiology and Immunology, Department of Pathology, University of Utah School of Medicine; Salt Lake City, UT 84112, USA

[2]Department of Biochemistry, University of Utah School of Medicine; Salt Lake City, UT 84112, USA

[3]Department of Immunology and Microbiology, School of Life Sciences, Southern University of Science and Technology; Shenzhen, Guangdong 518055, China

[4]Department of Microbiology, Harvard Medical School; Boston, MA 02115, USA

[5]Department of Cancer Immunology and Virology, Dana-Farber Cancer Institute; Boston, MA 02115, USA

*Corresponding author

Email: jarrod.johnson@path.utah.edu

Short title:

Disruption of HIV-1 cores triggers cGAS sensing of reverse transcripts

Abstract:

Retroviruses can be detected by the innate immune sensor cyclic GMP-AMP synthase (cGAS), which recognizes reverse-transcribed DNA and activates an antiviral response. However, the extent to which HIV-1 shields its genome from cGAS recognition remains unclear. To study this process in mechanistic detail, we reconstituted reverse transcription, genome release, and innate immune sensing of HIV-1 in a cell-free system. We found that wild-type HIV-1 capsids protect their genomes from cGAS even after completion of reverse transcription. Viral DNA could be “deprotected” by thermal stress, capsid mutations, or reduced concentrations of inositol hexakisphosphate (IP6) that destabilize the capsid. Strikingly, capsid inhibitors also disrupted viral cores and dramatically potentiated cGAS activity, both in vitro and in cellular infections. Our results provide biochemical evidence that the HIV-1 capsid lattice conceals the genome from cGAS and that chemical or physical disruption of the viral core can expose HIV-1 DNA and activate innate immune signaling.

Keywords:

DNA sensing; in vitro reverse transcription; capsid inhibition; innate immunity; HIV; cGAS; STING; IRF3; interferon; lenacapavir

Introduction

HIV-1 encapsidates its RNA genome and the viral enzymes necessary for replication within a conical capsid comprising ~1200 copies of the CA protein. Following viral fusion with a target cell membrane, the capsid and its contents (collectively known as the "core") are released into the cytosol. This initiates reverse transcription, converting two copies of the single-stranded RNA genome into one copy of double-stranded DNA (dsDNA). Reverse transcription is thought to proceed inside an intact, or largely intact, capsid as the viral core is trafficked from the cell surface to the nucleus[1–4]. Thus, it is presumed that HIV-1 shields the viral genome from innate immune sensors in the cytosol[5,6]. Uncoating and genome release occurs only moments before integration into host chromatin in the nucleus[4,7], although under some conditions retroviral capsids fail to completely protect reverse transcribed viral DNA, permitting its detection in dendritic cells and macrophages and the downstream induction of interferon (IFN) and inflammatory cytokines[6,8–12]. Mechanistic studies of HIV-1 sensing have remained challenging, however, because detection of reverse transcripts is a rare event that happens deep within these specialized cells.

Cyclic GMP-AMP synthase (cGAS) is the primary innate immune sensor that detects retroviral DNA[8,11]. Upon binding dsDNA in a sequence-independent manner, cGAS synthesizes the dinucleotide second messenger 2′3′-cyclic GMP-AMP (cGAMP), which binds and activates the adapter protein Stimulator of IFN genes (STING). STING then promotes downstream antiviral activities, including activation of the transcription factors IRF3 and NF-κB, which translocate to the nucleus and drive expression of type I and type III IFN[13,14]. IFN is rapidly secreted from the cell and initiates autocrine or paracrine signaling through IFN receptors. This upregulates hundreds of IFN-stimulated genes (ISGs), many of which can potently restrict HIV-1 infection[15–18]. Capsid structural integrity apparently influences the degree to which cGAS recognizes viral DNA, as specific CA mutations and CA-binding proteins are linked with

increased or decreased IFN responses during infection[5,6,11,12,19–24]. However, the parameters that regulate exposure of viral DNA and its detection by cGAS remain unclear.

Here, we have established a cell-free system for studying the essential steps in cGAS-mediated sensing of HIV-1. We find that wild type HIV-1 capsids remain stable and protect their genomes from cGAS detection, even several days after initiating reverse transcription. We also identified conditions and drug treatments that "deprotected" viral genomes and increased cGAS activity in vitro and in cells. Thus, the HIV-1 capsid is a molecular cloak that shields the viral genome from innate immune sensing.

Results

Reconstitution of HIV-1 innate immune sensing in vitro

The discovery that HIV-1 viral capsids are stabilized by IP6 has facilitated biochemical studies of endogenous reverse transcription and host-virus interactions[3,25–27]. We sought to extend these methods to study the physical and biochemical principles that control cGAS-mediated detection of reverse transcripts. To perform efficient endogenous reverse transcription (ERT), we permeabilized the viral membrane using the pore-forming peptide melittin, stabilized viral capsids in buffers that contained IP6 and ribonucleotides at the physiological levels observed in macrophages, and provided dNTP substrates for reverse transcription (Fig. 1A). Samples were then incubated with recombinant human cGAS to determine how efficiently the ERT products activated cGAS to produce cGAMP. cGAS activation levels were compared to those produced by a range of naked plasmid DNA concentrations. Relative DNA levels were measured by quantitative PCR (qPCR) detection of plasmid and full-length HIV-1_{SG3} genomes with primer sets that detected early, intermediate, and late reverse transcripts, and the equivalent DNA segments in the plasmid control (Fig. 1B). ERT was highly efficient, as previously reported[3], yielding roughly 0.5 copies of late RT products per input viral core, with

two copies of early and intermediate products for every copy of late RT (as predicted based on the number of primer binding sites present in the plasmid and viral genomes). As expected, plasmid DNA strongly activated cGAS in a concentration-dependent fashion. However, the HIV-1 ERT samples did not activate cGAS, suggesting that the viral DNA remained protected inside the capsid (Fig. 1C).

Performing ERT and cell-free sensing assays in two stages allowed us to uncouple parameters that influence ERT from parameters that impact cGAS activity (Fig. 1A). Viral cores that successfully completed RT were destabilized by limited heat treatment, which exposed the viral genome to cGAS (Fig. 1D). In contrast, heat treatment of plasmid control samples did not increase cGAS activity (S1 Fig A-C), reinforcing the idea that viral DNA is protected by the capsid.

HIV capsid stability can also be modulated by IP6[25,26] or by mutations in CA[3,28–32]. We therefore tested the effects of both variables on cGAS sensing of ERT products. Reducing IP6 from the cellular 40 μM concentration[33] to 0.4 μM increased cGAS detection of viral DNA by ~10-fold (Fig. 1E). cGAS sensing was similarly altered by CA mutations that either stabilize (E45A) or destabilize (Q63/67A) capsids[3,28]. Specifically, we observed that the destabilizing Q63/67A mutant enhanced cGAS activation (normalized for cDNA levels), particularly as IP6 levels were reduced (Fig. 1F,G). Conversely, the stabilizing E45A CA mutation reduced cGAS activation, resulting in limited cGAMP production even at very low IP6 levels. Both stabilized and destabilized capsid mutants were less infectious than wild type (wt) HIV-1 when pseudotyped reporter viruses were compared in THP-1 monocytic cells (S1 Fig. D). Our in vitro results indicate that capsid stability can modulate cGAS recognition, with stable capsids functioning to protect viral DNA from cGAS recognition better than unstable capsids.

Capsid inhibitors trigger viral core disruption and cGAS activation in vitro

Given that capsid stability regulates innate immune detection of HIV-1, we hypothesized that we could exploit chemical disruption of the capsid to unmask cGAS sensing of reverse transcripts. Consistent with this idea, the small molecule capsid inhibitor, PF74, can increase innate immune sensing of HIV-1 in cell lines, although this inhibitor has relatively low affinity for the capsid and does not completely block infection, even at micromolar concentrations[5,34]. Advances in drug development have led to Lenacapavir/Sunlenca (LEN), an FDA-approved capsid inhibitor that is 1000-fold more potent than PF74 at blocking HIV infection[35,36]. LEN is thought to work, at least in part, by flattening and rigidifying patches of the conical CA lattice, thereby inducing ruptures in the capsid[3,37]. We therefore tested whether LEN could "expose" viral reverse transcripts for detection in our vitro system.

We performed time course experiments to track production of reverse transcripts relative to naked plasmid DNA and again observed robust recombinant cGAS activity for plasmid, but not for ERT samples, even though levels of the plasmid control DNA and ERT DNA (16 h) were comparable (Fig. 2A). However, addition of LEN dramatically increased cGAS activation in the virus samples at late time points when dsDNA accumulated (Fig. 2A, lower panel). After 16 h of ERT in our standard assay conditions, LEN increased cGAS detection of HIV-1 greater than 10-fold, and this effect was specific for the ERT products because LEN did not alter cGAS sensing of naked plasmid DNA.

To determine whether cGAS activity from HIV-1 samples incubated with LEN depended on reverse transcription, we performed ERT and cGAS reactions with increasing concentrations of the reverse transcriptase inhibitor efavirenz (EFV). We confirmed that EFV blocked RT product formation in a dose-dependent manner as expected (Fig. 2B, top panel). In parallel, EFV treatments also reduced LEN-dependent cGAMP production, implying that cGAS activation was the direct result of viral DNA sensing in those reactions (Fig. 2B, bottom panel). Similar effects were observed for two other treatments that blocked ERT; omitting dNTPs or introducing

a point mutation that inactivated reverse transcriptase (D185A) (Fig. 2B). Dropout experiments confirmed that, as expected, LEN-dependent cGAS sensing of HIV-1 RT products also required virion permeabilization (mellitin), ERT ($MgCl_2$ and IP6), and enzymatic cGAMP production (NTPs and cGAS) (S2 Fig. A-E). cGAS sensing was also triggered by the LEN analog, GS-CA1[35], and by the weaker PF74 inhibitor[38], which all target the same capsid binding pocket[36,39] (S2 Fig. F,G).

We next assessed the specificity of the LEN effects by testing activity against CA mutations that inhibit LEN binding and confer drug resistance[36,40]. Control experiments confirmed that the M66I and Q67H/N74D CA mutations conferred LEN resistance to reporter virus infection of THP-1 cells, as expected (S3 Fig. A). In vitro, HIV-1 cores carrying these LEN resistance mutations completed ERT at normal levels (Fig. 3A). However, these mutant virions did not stimulate cGAS activity when treated with LEN (Fig. 3B). In control experiments, heat treated mutant capsids stimulated cGAS normally, indicating that their DNA was detectable when exposed by other methods of capsid disruption (S3 Fig. B). These experiments demonstrate that LEN must bind the viral capsid to stimulate cGAS activity.

During a normal infection, the viral DNA must eventually exit the capsid to integrate into the host genome, but the mechanism of release (termed “uncoating”) is not well understood. In particular, it is not yet clear whether uncoating occurs stochastically, is driven by pressure caused by accumulation of viral dsDNA, or is facilitated by host factors. To determine whether prolonged incubation of viral cores might lead to capsid permeability and genome release, we ran ERT reactions and incubated the samples for 16, 24, 48, and 72 h at 37°C and then performed cGAS DNA sensing assays. DNA product levels were quite stable across these time points (Fig. 3C), yet cGAS activation increased modestly (3- to 4-fold) from 16 to 72 h, indicating that ERT products became more exposed over time (grey bars, Fig. 3D). Nevertheless, even 72 h after reverse transcription was initiated, cGAS activity was still further stimulated (~3-fold) by LEN treatment, indicating that capsids provide stable protection of viral DNA in vitro for days

after completion of reverse transcription. Together, these data indicate that: 1) the HIV-1 capsid
150 protects the viral genome from innate immune sensing, and 2) pharmacological disruption of the capsid enables cGAS detection of reverse transcripts.

LEN treatment triggers cellular sensing of HIV-1 via the cGAS-STING pathway

We extended our findings to cellular models of HIV infection. In vitro, LEN-dependent
155 cGAS activation by ERT reactions exhibited biphasic behavior (Fig. 4A). At high concentrations (>30 nM), LEN inhibited reverse transcription (Fig. 4A, top panel) and cGAS activation was therefore prevented because dsDNA was not present for detection[3]. Lower LEN concentrations (1–10 nM) stimulated cGAS activation in a dose dependent fashion because reverse transcription proceeded, and viral cores were increasingly disrupted, triggering cGAS activation
160 (Fig. 4A, bottom panel). To determine whether these effects were recapitulated in the context of a viral infection, we tested the effects of different LEN levels on THP-1 cells treated with HIV-1-GFP and tracked both infectivity and innate immune activation, measured by stimulation of two different ISGs: ISG15 and SIGLEC1 (Fig. 4B,C). Our experiments demonstrated that the LEN effects observed in cells mirrored those in our in vitro system, with high LEN levels inhibiting
165 cGAS activation, presumably by blocking reverse transcription, but lower LEN levels stimulating ISG15 and SIGLEC1 expression (Figs. 4C; S4 Fig. A,B), at concentrations that matched the levels that stimulated cGAS activity in vitro (1–10 nM). In contrast, LEN treatments did not stimulate ISG expression upon infection by the LEN-resistant mutants M66I and Q67H/N74D, demonstrating the specificity of drug activity in cells (S4 Fig. C). We note, however, that
170 although the M66I mutation reduced viral infectivity, the mutant virus induced ISG expression at levels that were similar to wt HIV-1, consistent with the idea that this mutation reduces viral fitness owing to capsid structural defects[41,42]. Most importantly, our data indicate that LEN can stimulate innate immune sensing of incoming wt HIV-1 particles, at concentrations that still block infection.

175 To determine whether LEN-triggered innate immune activation occurred through the canonical cGAS/STING pathway, we employed the lentiCRISPR system[43] to knock out the key pathway components, cGAS, STING, or IRF3. Pools of THP-1 monocytic cells were transduced with lentiCRISPR vectors, expanded for two weeks under antibiotic selection, and target protein loss was confirmed by immunoblot (Fig. 4D). As expected, HIV-1 infection was eliminated by
180 LEN treatment (10 nM), but was not affected by loss of cGAS, STING, or IRF3 (Fig. 4E). However, loss of each innate immune protein substantially reduced ISG protein expression, both in the absence of capsid inhibition and in the presence of LEN (Fig. 4E,F). Thus, LEN stimulates innate immune recognition of HIV-1 through the canonical cGAS/STING pathway.

Recent work has suggested that an additional factor, polyglutamine-binding protein 1
185 (PQBP1), helps to license cGAS activity during HIV-1 infection, through its capacity to link cGAS to the viral capsid[23,44]. In our cell-free system, full-length recombinant PQBP1 protein did not enhance cGAS activity, either alone or together with HIV-1 (S4 Fig. D,E). Similarly, we observed that loss of PQBP1 did not alter viral infectivity or reduce innate immune sensing of HIV-1 in myeloid cells, using two independent guide RNAs to knockout PQBP1 expression (S4 Fig. F-I).
190 In contrast, removal of cGAS (positive control) ablated ISG responses to HIV-1-GFP in the presence or absence of the integration inhibitor elvitegravir (S4 Fig. G,I).

Finally, we evaluated whether capsid inhibition could facilitate innate immune responses while blocking HIV-1 infection in primary human myeloid cells. Human monocyte-derived dendritic cells (MDDCs) and monocyte-derived macrophages (MDMs) can be infected by HIV-1,
195 particularly when the lentiviral accessory protein Vpx is provided in trans to overcome SAMHD1-mediated restriction in MDDCs[45,46]. In some cases, MDDCs and MDMs can respond to HIV-1 by producing type I IFN and other inflammatory cytokines[6,9,11,12,47,48]. We infected MDDCs and MDMs from four unique donors with HIV-1-GFP (Fig 4G,I), and found that 3–30 nM concentrations of the LEN analog, GS-CA1, efficiently blocked infection in MDDCs and MDMs.
200 Importantly, however, ISG15 activation was still sustained at these inhibitory concentrations

(Fig. 4H,J). Hence, potent LEN-class capsid inhibitors can simultaneously prevent HIV-1 infection while still maintaining robust innate immune responses in primary human myeloid cells.

Discussion

205 IFN creates strong selective pressure on HIV-1 during sexual transmission and during viral rebound in response to withdrawal of antiviral therapy[49,50]. It is therefore critical to understand how HIV is sensed by the innate immune system. Multiple innate immune sensors can contribute to IFN and inflammation during HIV-1 infection[47,48,51–55], but cGAS activation is increasingly appreciated as a driver of protective anti-HIV immune responses. For example, this
210 pathway is robustly activated in myeloid cells from elite controllers[56,57], and myeloid cell programming of polyfunctional CD8+ T cells is critical for control of infection[58,59]. However, precisely how viral DNA is released from the capsid to activate cGAS has not been well characterized.

To begin to address this issue, we have reconstituted endogenous reverse transcription,
215 capsid destabilization, and innate immune sensing of HIV-1 in a cell-free system. We find that HIV-1 capsids protect reverse transcripts from detection by cGAS, and that this protection can last for days after reverse transcription is complete. This protection appears to be mediated by intact, or largely intact capsids because cGAS recognition increases dramatically when capsids are disrupted by heat, reduced IP6 concentrations, or destabilizing mutations in the viral capsid.
220 Our observation that capsid integrity and stability can strongly modulate cGAS-mediated detection of HIV-1 is consistent with a growing body of literature indicating that the capsid sequence has a substantial impact on sensitivity to innate immune sensors[6,11,12,19,21], and that IP6 perturbations or improper capsid formation can promote cGAS activation[5,20]. We suggest that our in vitro system can be useful in characterizing these effects, and also in determining
225 how host factors promote capsid uncoating and cDNA exposure.

Most importantly, we find that capsid inhibitors of the LEN class can promote HIV-1 DNA genome exposure and cGAS activation in vitro, in THP-1 cells, and primary human myeloid cells. In the THP-1 case, and presumably also in primary myeloid cells, cGAS activation by reverse transcription products leads to innate immune activation via the canonical STING pathway. However, we have not yet identified conditions that lead to LEN-induced IFN production in CD4+ T cells, suggesting that additional host circuitry might be required to unleash this response in the main target cells of HIV[60,61].

In summary, our experiments are consistent with a model in which viral cores enter the cytoplasms of myeloid cells, and reverse transcription normally proceeds inside an intact or largely intact capsid, where the viral cDNA is protected from innate immune sensors[1,6,12,22]. However, in the presence of LEN, accumulated reverse transcripts can become exposed by drug-induced capsid rupturing, enabling viral DNA detection and downstream activation of IFN production via the cGAS-STING-IRF3 pathway (S1 Movie.). Importantly, LEN can inhibit multiple steps in the virus life cycle at different drug concentrations, including virus assembly and a step corresponding to nuclear entry or a later pre-integration step, with the latter being the most potent block to infection in cultured cells (0.5–5 nM)[35]. Reverse transcription can also be inhibited, but this requires drug concentrations (≥25 nM) that are much higher than the protein-adjusted EC95 required to inhibit HIV-1 replication (~4 nM)[35,36]. In our studies, LEN promotes cGAS activation at concentrations that parallel those that block nuclear entry and/or integration (1–10 nM, see Fig. 4), and we therefore speculate that the most potent mechanism of drug action may be associated with premature genome release. Our experiments also indicate that, at least in culture, cGAS activation can occur under conditions where viral infectivity is suppressed but innate immune responses are maintained. We therefore speculate that the drug-dependent effects we observe in cultured cells might be harnessed to potentiate vaccination responses under conditions where viral replication is blocked while antiviral immunity remains engaged.

Acknowledgments:

We thank members of the Johnson and Sundquist laboratories for helpful discussions as we developed this project. We thank Miguel Pereira for improvements to our virus purification protocol, which removed trace amounts of DNA contaminants and increased signal to noise in our cGAS assay. Oligonucleotides were synthesized by the University of Utah DNA/Peptide Core Facility, sequencing of constructs was performed at the University of Utah DNA sequencing Core Facility, and flow cytometry was performed at the University of Utah Flow Core. We acknowledge funding from National Institutes of Health grant U54 AI170856 (to WIS and JSJ), R56 AI174930 (JSJ), 1DP2GM146250-01 (PJK), and grants from the Pew Biomedical Scholars program (PJK), and the Burroughs Wellcome Fund PATH program (PJK). W.Z. was supported in part through a Charles A. King Trust Postdoctoral Fellowship. The funders had no role in study design, data collection, and interpretation, or the decision to submit the work for publication.

Author contributions:

Conceptualization: WIS, JSJ

Methodology: TMS, LMA, DC, WZ, PJK, WIS, JSJ

Investigation: TMS, LMA, JAP, DAM, DC, WZ, JSJ

Funding acquisition: PJK, WIS, JSJ

Project administration: PJK, WIS, JSJ

Supervision: PJK, WIS, JSJ

Writing – original draft: JSJ

Writing – review & editing: all authors

Competing interests:

The authors declare no competing interests.

280 **Methods**

Cell lines and blood-derived dendritic cells

To generate MDDCs and MDMs, we acquired leukocytes from de-identified normal human donors from ARUP Blood Services, Sandy, UT, USA, similar to previously described
285 methods[62]. We cannot report on the sex, gender, or age of the donors since the samples were de-identified and donors remain anonymous. Peripheral blood mononuclear cells (PBMCs) were layered over Ficoll-Paque Plus (GE Healthcare). CD14+ monocytes from PBMC buffy coats were isolated with anti-human CD14 magnetic beads (Miltenyi) and cultured in RPMI containing 10% heat-inactivated fetal bovine serum (FBS, Gibco), 50 U/ml penicillin, 50 µg/ml streptomycin
290 (pen/strep, Thermo Fisher), 10 mM HEPES (Sigma), and 55 µM 2-Mercaptoethanol (Gibco). We tested multiple lots of FBS to identify batches that lead to minimal baseline induction of activation markers over the course of MDDC differentiation. MDDCs were derived in the presence of recombinant human GM-CSF (Peprotech) at 10 ng/ml and IL-4 at 50 ng/ml. MDMs were derived using recombinant human M-CSF (Peprotech) at 20 ng/ml. Fresh media and
295 cytokines were added to cells (40% by volume) one day after CD14+ cell isolation. On day 4, MDDCs were collected, resuspended in fresh media with cytokines used for infection or stimulation such that experimental end points would fall on day 6. MDM cultures were replenished with fresh media on day 4, then infected or stimulated on day 5 so that experimental end points would fall on day 7 after isolation. MDDC and MDM experiments were performed
300 using biological replicates from blood-derived cells from multiple individual donors as indicated in the figure legends.

We cultured 293FT cells (immortalized from a female fetus, Life Technologies Cat# R70007, RRID: CVCL_6911) in Dulbecco's modified Eagle's medium (DMEM, Thermo Fisher) supplemented with 10% heat-inactivated FBS, pen/strep, 10mM HEPES, and 0.1 mM MEM non-essential amino acids (Thermo Fisher). THP-1 cells (derived from a male patient with acute monocytic leukemia, ATCC) were cultured in RPMI (Thermo Fisher) containing 10% FBS, pen/strep, 10 mM HEPES, and 2-Mercaptoethanol.

Cell lines were used at early passage numbers and fresh stocks were thawed every 1–2 months. Cell cultures were routinely tested for mycoplasma contamination every 6 months. All cells were maintained at 37°C and 5% CO_2.

Plasmids and mutagenesis

For endogenous reverse transcription reactions full-length $pHIV_{SG3}$ (ΔEnv) was acquired from the NIH AIDS Reagent Program (Catalog # 11051). HIV-1-GFP is derived from an HIV-1 NL4-3 vector that has been used to study immune responses in myeloid cells lines and primary human MDDCs[12]. HIV-1-GFP is env- vpu- vpr- vif- nef-, with the GFP open reading frame in place of nef. We generated virus like particles packaging Vpx from the plasmid pSIV3+ (based on SIVmac251, GenBank acc. no. M19499), which has been described previously[63]. These and all other plasmids used in this study are listed in the Supplementary Table (S1 Table.) and have been made available through Addgene. Target sequences for lentiCRISPR vectors are also provided (S1 Table.). All lentiviral constructs were transformed into Stbl3 bacteria (ThermoFisher) for propagation of plasmid DNA. The coding sequence for full-length human PQBP1 was synthesized as a GBlock gene fragment (IDT) and cloned into pCA528 by Gibson assembly. All plasmids were prepped and purified through PureLink HiPure Plasmid Maxiprep Kits (Invitrogen).

Virus and vector production

330 Reporter viruses, recombinant lentiviral vectors, and Vpx-containing virus-like particles, were produced by transient transfection in 293FT cells, similar to previously described methods (Johnson et al., 2018). Briefly, the day before transfection, cells were seeded onto poly-L-lysine-(Sigma) coated 15 cm plates to be ~70% confluent at the time of transfection. Cells were transfected with a total of 22–25 µg DNA using PEImax (Polysciences, Inc.). Each batch of PEI
335 was titered to identify the optimal ratio of DNA:PEI for transfection (which was typically close to 1:2). To produce wt SG3ΔEnv and mutant virions, a single plasmid was transfected into 293FT cells. For HIV-1-GFP reporter viruses, we transfected 19.1 µg of the HIV cassette and 3.4 µg of pCMV-VSV-G. For lentiCRISPR vectors, we transfected 13.5 µg of the transgene plasmid, 8 µg of psPax2 helper plasmid, and 3.5 µg pCMV-VSV-G. Virus-like particles containing Vpx were
340 produced by transfecting 19.1 µg pSIV3+ and 3.5 µg pCMV-VSV-G. The morning after transfection, cells were washed once and replenished with 30 ml of fresh media. To remove exosome contaminants in virus preparations to be used for ERT and cell-free sensing reactions, we used media that contained FBS that had been depleted of exosomes (ultracentifugation for 16 h at 100,000 rcf). Supernatants were harvested 36–48 h after replenishing media and then
345 passed through 0.45 µm syringe filters (Corning) to remove debris.

To further purify wt and mutant SG3ΔEnv virions used for ERT reactions and cell-free sensing assays, virus supernatants (30 ml) were treated for 1 h at 37°C with 2500 U ultrapure benzonase nuclease (Sigma, E8263-25KU), subtilisin protease at 200 µg/ml (Sigma), and
350 additional $MgCl_2$ (1 mM) to remove trace amounts of plasmid and genomic nucleic acid contaminants[64]. Protease activity was then quenched by adding 10 µl of 15 mg/ml PMSF. HIV-1-GFP wt and mutant virions were treated in a similar fashion except were not treated with subtilisin and PMSF. Supernatants were then layered over a 20% sucrose cushion (in PBS) and

concentrated by ultracentrifugation by spinning in 15 x 89 mm ultraclear tubes (Beckman) at 28 K rpm for 2 h at 4°C in an SW32 swing-bucket rotor (Beckman). SG3ΔEnv virions were thoroughly resuspended using 500 µl Hepes/Salt buffer per tube. HIV-1-GFP wt and mutant virions and lentiCRISPR vectors were resuspended in 1 ml of complete RPMI media. With high titer stocks of HIV-1-GFP and lentiCRISPR vectors we occasionally observed insoluble virus aggregates that we clarified from virion preparations by low-speed centrifugation at 300 rcf for 3 min at 4°C. Purified viral stocks were frozen at −80°C, titered by p24 ELISA (Express Bio), and used as indicated below.

Bacterial expression and purification of recombinant human cGAS

Full-length human cGAS (aa 1–522, HGNC:21367) was produced and purified as previously described[65,66]. Briefly, human cGAS was expressed as a fusion protein with a 6×His-SUMO2 tag in *Escherichia coli* (*E. coli*) BL21-RIL DE3 (Agilent) bacteria harboring a pRARE2 tRNA plasmid. Initial cultures were grown in 30 ml of MDG media (25 mM Na_2HPO_4, 25 mM KH_2PO_4, 50 mM NH_4Cl, 5 mM Na_2SO_4, 2 mM $MgSO_4$, 0.5% glucose, 0.25% aspartic acid, 100 µg/ml ampicillin, 34 µg/ml chloramphenicol, and trace metals) to an OD_{600} of ~0.05. These cultures were then used to seed 2 L M9ZB media (7.8 mM Na_2HPO_4, 22 mM KH_2PO_4, 18.7 mM NH_4Cl, 85.6 mM NaCl, 2 mM $MgSO_4$, 0.5% glycerol, 1% Casamino acids, 100 µg/ml ampicillin, 34 µg/ml chloramphenicol, and trace metals) at 37°C until an OD_{600} of ~2.5–3.0 was reached. The cultures were supplemented with IPTG (0.5 mM) and incubated at 16°C for an additional 12–16 hours. Next, bacteria were pelleted, flash-frozen in liquid nitrogen, and stored at −80°C until further purification.

Bacterial pellets with cGAS fusion proteins were resuspended in lysis buffer (20 mM HEPES-KOH pH 7.5, 400 mM NaCl, 10% glycerol, 30 mM imidazole, 1 mM dithiothreitol (DTT) and subsequently lysed by sonication. The supernatant containing cGAS was collected for initial

380 purification using Ni-NTA (Qiagen) resin and gravity chromatography. Eluted 6×His-SUMO2-cGAS proteins were supplemented with ~250 µg of human SENP2 protease to remove the His-SUMO2 tag and treated in dialysis buffer (20 mM HEPES-KOH pH 7.5, 300 mM NaCl, 1 mM DTT) at 4°C for ~12 hours. The dialysate was purified by using heparin HP ion exchange (GE Healthcare) and eluted with a 300–1000 mM NaCl gradient. Full-length untagged cGAS protein
385 was then ultimately purified using size-exclusion chromatography via a 16/600 Superdex S75 column (GE Healthcare). Purified cGAS was concentrated to ~10 mg/ml in storage buffer (20 mM HEPES-KOH pH 7.5, 250 mM KCl, 1 mM TCEP), flash-frozen in liquid nitrogen, and stored as aliquots at −80°C for biochemical experiments.

390 **Bacterial expression and purification of recombinant human PQBP1**

Full-length human PQBP1 (HGNC:9330) was cloned into pCA528 for bacterial expression as a $(His)_6$-SUMO-fusion protein. $(His)_6$-SUMO-PQBP1 was expressed in BL21 RIPL cells grown in 2xYT media. Transformed cells were initially grown for 3–6 h at 37°C to an OD600 of 0-4–0.6, IPTG (Isopropyl ß-D-1-thiogalactopyranoside) was added to final concentration of 0.5
395 mM to induce recombinant protein expression and cells were cultured for an additional 4 h. Cells were harvested by centrifugation at 6,000 x g and cell pellets were stored at −80°C.

All purification steps were carried out at 4°C except where noted. Frozen cell pellets were thawed and resuspended in lysis buffer: 50 mM Tris (pH 8.0 at 23 °C), 500 mM NaCl, 2 mM
400 Imidazole, 0.5 mM EDTA, supplemented with lysozyme (25 µg/mL), PMSF (100 µM), Pepstatin (10 µM), Leupeptin (100 µM), Aprotinin (1 µM), and DNase I (10 µg/mL). Cells were lysed by sonication and lysates were clarified by centrifugation at 40,000 x g for 45 min. Clarified supernatant was filtered through a 0.45 µM PES syringe filter and incubated with 10 mL of cOmplete His-Tag purification beads (Roche) for 1 h with gentle rocking. Beads were washed

405 with 150 mL unsupplemented lysis buffer. PQBP1 fusion protein was eluted with 50 mL of lysis buffer supplemented with 250 mM Imidazole.

Eluted proteins were treated with 100 µg His_6-ULP1 protease overnight in 6–8 k MWCO dialysis bags while dialyzing against 2 x 2 L of 25 mM Tris (pH 8.0 at 23 °C), 50 mM NaCl, 1 mM
410 TCEP. The dialysate was purified by Q Sepharose chromatography (HiTrap Q HP 5 mL; Cytiva Life Sciences) with a linear gradient elution from 50–1000 mM NaCl. Fractions containing processed fusion proteins were then passed over 5 mL of cOmplete His-Tag purification beads to remove residual uncleaved His_6-Sumo-PQBP1 and His_6-Sumo cleaved tag. The sample was then placed in 6–8 k MWCO dialysis bag while dialyzing against 2 x 2 L of 25 mM Tris pH (8.0 at
415 23 °C), 50 mM NaCl, 1 mM TCEP. The dialysate was purified by Heparin Sepharose chromatography (HiTrap Heparin HP 5 mL; Cytiva Life Sciences) with a linear gradient elution from 50–1000 mM NaCl. PQBP1 rich fractions were concentrated and purified by Superdex 75 gel filtration chromatography (120 mL;16/600; Cytiva Life Sciences) in 50 mM Tris (pH 8.0 at 23 °C) 150 mM NaCl, 1 mM TCEP. Highly pure PQBP1 fractions were pooled, concentrated to ~200
420 µM, aliquoted and stored at −80°C.

Endogenous Reverse Transcription (ERT)

Experimental conditions for ERT reactions were optimized from existing protocols[3,27]. Briefly, we diluted SG3ΔEnv virions to 50 nM CA in reaction mixtures that contained 50 mM Tris
425 (pH 7.5 at 37C), 100 nM NaCl, 1.65 mM $MgCl_2$, 40 µM IP6, 1mg/ml BSA, 10 µg/ml melittin (Sigma), ribonucleoside triphosphates (NTPs) (Promega), and deoxynucleotide triphosphates (dNTPs) (Promega). NTP concentrations were chosen to match levels reported in macrophage cytoplasm[67] and were as follows: ATP: 1.124 mM; GTP: 323 µM; UTP: 173 µM; CTP: 25 µM. The concentration of Mg2+ was chosen to match the total concentration of NTPs in the reaction
430 (1.65 mM) and we validated empirically that this optimized ERT yield. dNTP concentrations

were previously established[3,68] and were as follows: dATP: 5.2 μM; dGTP: 4.6 μM; dCTP: 6 μM; dTTP: 8 μM. We determined that ERT reactions could proceed using a range of melittin concentrations, and we chose 10 μg/ml for our standard conditions since higher concentrations of melittin (>25 μg/ml) were found to inhibit cGAS activity in the second stage of the assay. Reducing the concentration of melittin below 2.5 μg/ml led to reduced IP6 dependence (i.e. late RT products were produced even in the absence of IP6), suggesting that at lower concentrations of melittin, the membrane was incompletely stripped from the viral core and capsid stability was no longer influenced by IP6.

For plasmid comparisons in ERT reactions, we used the pSG3Δenv plasmid diluted to match the expected copy number for late reverse transcription products from HIV-1_{SG3} (typically 20–40 ng/reaction). Plasmid and HIV-1_{SG3} virions were incubated under identical conditions as described in the figure legends. After 16 h ERT incubations, column-based purification, and qPCR determination of DNA copy number from eluates (described below), plasmid copy numbers ranged from 5 M to 10 M copies per qPCR reaction. ERT reactions were performed in 60 μl volumes and held at 37ºC in a ProFlex thermocycler (Thermo Fisher) for the times indicated in the figure legends and cooled to room temperature prior to downstream studies. Samples from the same ERT reactions were divided into cGAS sensing assays or used for qPCR analysis of DNA yield.

Cell-free cGAS sensing assay

Samples from ERT reactions were diluted 50- to 100-fold into cell-free cGAS assay buffers that were similar to standard ERT reaction mixtures, but lacked melittin (50 mM Tris pH 7.5, 100 nM NaCl, 40 μM IP6, 1mg/ml BSA, NTPs, and 2.2 mM $MgCl_2$). Full length recombinant human cGAS was added at 10 nM. BSA was not required for DNA product formation in ERT reactions but was critical to observe a cGAMP signal above the limit of detection in cell-free

cGAS assays. Product formation in the cGAS assay was exquisitely sensitive to Mg^{2+} concentration (S1 Fig. E). Although we observed similar responses to HIV-1 + LEN over a range of Mg^{2+}concentrations (1.65 mM to 5 mM), our standard reaction conditions reported throughout the manuscript were performed using 2.2 mM $MgCl_2$ to ensure adequate signal to noise. Interestingly, higher concentrations of $MgCl_2$ (such as 10 mM) were associated with greater cGAS activity at baseline and reduced responsiveness to LEN. This effect is likely driven by two factors: 1) cations such as Mg^{2+} and Mn^{2+} support cGAS activity in vitro[69], and 2) at high concentrations, Mg^{2+} cations might disrupt capsid stability, by interfering with CA subunit interactions and/or by chelating IP6 away from the capsid, leading to loss of capsid integrity, genome release, and reduced responsiveness to LEN.

In some experiments, plasmid DNA or HIV-1 ERT samples were heat treated prior to incubation in cell-free cGAS assays. Aliquots from ERT reactions were transferred to new PCR tubes and incubated for 20 s in a ProFlex thermocycler at a range of temperatures (37ºC-62.5ºC). Samples were cooled to room temperature before diluting into cGAS assays. cGAS assay sample volumes typically ranged from 100-200 µl and reactions were incubated for 8 h at 37ºC in a thermocycler. Samples were held at 4C for short term storage or frozen at −80°C. cGAMP levels from cGAS assays were determined by ELISA (Arbor Assays) according to the manufacturers' instructions. Reaction mixtures were diluted 1:2 in assay buffer and compared to a standard curve using purified 2'3'-cGAMP. Data were analyzed and plotted using GraphPad Prism software. For dose curves comparing responses to LEN, GS-CA1, or PF-74, heat maps were generated using Morpheus (Broad Institute).

Quantitative PCR analyses

For each ERT reaction, 30 µl of sample was purified using a Qiaquick PCR purification kit (Qiagen) and eluted from the column in 75 µl elution buffer (Qiagen). qPCR reactions were

performed and analyzed in triplicate. Standard curves for ERT products were generated by using a 10-fold dilution series of the pSG3Δenv plasmid that were run in parallel with
485 experimental samples and tested using early, intermediate, and late RT primers. Each qPCR sample was comprised of 2.5 µl elution product from purified ERT reactions, 2X Sybr Green master mix (Abclonal), 1 µl of primers (2 µM stock), and water to a total of 10 µl reaction volume. qPCR reactions were performed on a QuantStudio 3 (Thermo Fisher) and analyzed using GraphPad Prism software. For experiments measuring plasmid DNA as a control, plasmid
490 copy numbers determined for each primer set were multiplied by a factor of 1.5 to account for the length difference between the plasmid (14,788 bp) and the reverse transcribed viral genome (~9,730 bp) in order to plot base-adjusted copy number. At least twice as many copies of early and intermediate products are expected for every one copy of late RT in both the plasmid and HIV-1 full-length genome, based on the number of primer binding sites present in those target
495 sequences.

Flow cytometry

Infections with HIV-1-GFP reporter viruses were performed in 96 well plates as described previously[9,62]. Briefly, ~50,000 MDDCs, 25,000 MDMs, or 100,000 THP-1 cells were
500 seeded in 96 well plates and infected as described in the Figure legends with the indicated amounts of virus (typically 12.5 to 50 nM p24) in the presence of polybrene (0.5 – 5 µg/ml). For flow cytometry, 48 h after infection, MDDCs, MDMs, or THP-1 cells were washed with phosphate buffered saline (PBS, Corning) and then exposed to LIVE/DEAD violet (ThermoFisher) in PBS for 15 min at 4 °C in the dark. For intracellular staining using anti-human
505 ISG15-PE (R&D Systems) or SIGLEC1-647 (BD Biosciences), cells were then fixed and permeabilized using a cytofix/cytoperm kit (BD Biosciences) and stained according to the manufacturers' instructions. Antibody staining was performed for 30 min at room temperature in the dark. Cells were washed and resuspended in PBS with 1% BSA and then analyzed on an

Attune flow cytometer (Thermo Fisher). Data were analyzed using FlowJo software (FlowJo
510 LLC). Heat maps were generated using Morpheus (Broad Institute).

CRISPR-mediated gene editing

THP-1 monocytic cells were modified by lentiCRISPR vectors as previously described[9]. Briefly, we transduced cells in 6-well cluster plates using 800,000 cells per well in 2 ml media
515 with polybrene (5 µg/mL) and concentrated lentiviral stocks (200 µl per well). Two days after transduction, cells were put under selection with puromycin (1 µg/ml, Invivogen) for 4 days and then puromycin was reduced to half-strength for maintenance. Cells were used for experiments beginning 2 weeks after selection. Disruption of target gene expression was confirmed by immunoblot using antibodies to detect cGAS, STING, IRF3, or PQBP1 compared to an actin
520 loading control (as listed in S1 Table.).

Immunoblotting

One million cells were spun down in 1.5 mL tubes and lysed in 150–200 µL SDS sample buffer (2% SDS, 50 mM Tris, 12.5 mM EDTA, plus Halt protease and phosphatase inhibitors
525 (Thermo Fisher)). Samples were sonicated using a microtip Branson sonifier (10–20, 1 s pulses on low output) and protein concentrations were determined using a reducing agent-compatible BCA assay (Thermo Fisher) according to the manufacturer's instructions. Equal amounts of protein (typically 15–20 µg) were loaded with LDS loading buffer (Life Technologies) and separated on 4–12% gradient poly-acrylamide Bolt Bis-Tris gels (Thermo Fisher). Proteins were
530 transferred to nitrocellulose membranes, blocked using 2.5% BSA (Roche) in Tris buffered saline (TBS) with 0.5% tween. Blots were incubated with primary antibodies, then corresponding fluorescent-conjugated anti-mouse or anti-rabbit secondary antibodies (LI-COR), and then fluorescent images were acquired using an Odyssey Imager (LI-COR). Blot images were analyzed using Image Studio Lite (LI-COR).

535 **References**

1. Zila, V., Margiotta, E., Turonova, B., Muller, T.G., Zimmerli, C.E., Mattei, S., Allegretti, M., Borner, K., Rada, J., Muller, B., et al. (2021). Cone-shaped HIV-1 capsids are transported through intact nuclear pores. Cell *184*, 1032-1046 e18. 10.1016/j.cell.2021.01.025.

540 2. Müller, T.G., Zila, V., Peters, K., Schifferdecker, S., Stanic, M., Lucic, B., Laketa, V., Lusic, M., Müller, B., and Kräusslich, H.-G. (2021). HIV-1 uncoating by release of viral cDNA from capsid-like structures in the nucleus of infected cells. eLife *10*, e64776. 10.7554/eLife.64776.

3. Christensen, D.E., Ganser-Pornillos, B.K., Johnson, J.S., Pornillos, O., and Sundquist, W.I.
545 (2020). Reconstitution and visualization of HIV-1 capsid-dependent replication and integration in vitro. Science *370*. 10.1126/science.abc8420.

4. Burdick, R.C., Li, C., Munshi, M., Rawson, J.M.O., Nagashima, K., Hu, W.S., and Pathak, V.K. (2020). HIV-1 uncoats in the nucleus near sites of integration. Proc Natl Acad Sci U S A *117*, 5486–5493. 10.1073/pnas.1920631117.

550 5. Sumner, R.P., Harrison, L., Touizer, E., Peacock, T.P., Spencer, M., Zuliani-Alvarez, L., and Towers, G.J. (2020). Disrupting HIV-1 capsid formation causes cGAS sensing of viral DNA. EMBO J *39*, e103958. 10.15252/embj.2019103958.

6. Rasaiyaah, J., Tan, C.P., Fletcher, A.J., Price, A.J., Blondeau, C., Hilditch, L., Jacques, D.A., Selwood, D.L., James, L.C., Noursadeghi, M., et al. (2013). HIV-1 evades innate
555 immune recognition through specific cofactor recruitment. Nature *503*, 402–405. 10.1038/nature12769.

7. Li, C., Burdick, R.C., Nagashima, K., Hu, W.-S., and Pathak, V.K. (2021). HIV-1 cores retain their integrity until minutes before uncoating in the nucleus. Proceedings of the National Academy of Sciences *118*, e2019467118. 10.1073/pnas.2019467118.

560 8. Gao, D., Wu, J., Wu, Y.T., Du, F., Aroh, C., Yan, N., Sun, L., and Chen, Z.J. (2013). Cyclic GMP-AMP synthase is an innate immune sensor of HIV and other retroviruses. Science *341*, 903–906. 10.1126/science.1240933.

9. Johnson, J.S., Lucas, S.Y., Amon, L.M., Skelton, S., Nazitto, R., Carbonetti, S., Sather, D.N., Littman, D.R., and Aderem, A. (2018). Reshaping of the Dendritic Cell Chromatin
565 Landscape and Interferon Pathways during HIV Infection. Cell Host Microbe *23*, 366-381 e9. 10.1016/j.chom.2018.01.012.

10. Yan, N., Regalado-Magdos, A.D., Stiggelbout, B., Lee-Kirsch, M.A., and Lieberman, J. (2010). The cytosolic exonuclease TREX1 inhibits the innate immune response to human immunodeficiency virus type 1. Nat Immunol *11*, 1005–1013. 10.1038/ni.1941.

570 11. Lahaye, X., Satoh, T., Gentili, M., Cerboni, S., Conrad, C., Hurbain, I., El Marjou, A., Lacabaratz, C., Lelievre, J.D., and Manel, N. (2013). The capsids of HIV-1 and HIV-2 determine immune detection of the viral cDNA by the innate sensor cGAS in dendritic cells. Immunity *39*, 1132–1142. 10.1016/j.immuni.2013.11.002.

12. Manel, N., Hogstad, B., Wang, Y., Levy, D.E., Unutmaz, D., and Littman, D.R. (2010). A cryptic sensor for HIV-1 activates antiviral innate immunity in dendritic cells. Nature *467*, 214–217. 10.1038/nature09337.

13. Yum, S., Li, M., Fang, Y., and Chen, Z.J. (2021). TBK1 recruitment to STING activates both IRF3 and NF-κB that mediate immune defense against tumors and viral infections. Proceedings of the National Academy of Sciences *118*, e2100225118. 10.1073/pnas.2100225118.

14. Liu, S., Cai, X., Wu, J., Cong, Q., Chen, X., Li, T., Du, F., Ren, J., Wu, Y.T., Grishin, N.V., et al. (2015). Phosphorylation of innate immune adaptor proteins MAVS, STING, and TRIF induces IRF3 activation. Science *347*, aaa2630. 10.1126/science.aaa2630.

15. Schoggins, J.W., Wilson, S.J., Panis, M., Murphy, M.Y., Jones, C.T., Bieniasz, P., and Rice, C.M. (2011). A diverse range of gene products are effectors of the type I interferon antiviral response. Nature *472*, 481–485. 10.1038/nature09907.

16. Johnson, J.S., De Veaux, N., Rives, A.W., Lahaye, X., Lucas, S.Y., Perot, B.P., Luka, M., Garcia-Paredes, V., Amon, L.M., Watters, A., et al. (2020). A Comprehensive Map of the Monocyte-Derived Dendritic Cell Transcriptional Network Engaged upon Innate Sensing of HIV. Cell Rep *30*, 914-931 e9. 10.1016/j.celrep.2019.12.054.

17. Kane, M., Zang, T.M., Rihn, S.J., Zhang, F., Kueck, T., Alim, M., Schoggins, J., Rice, C.M., Wilson, S.J., and Bieniasz, P.D. (2016). Identification of Interferon-Stimulated Genes with Antiretroviral Activity. Cell Host Microbe *20*, 392–405. 10.1016/j.chom.2016.08.005.

18. OhAinle, M., Helms, L., Vermeire, J., Roesch, F., Humes, D., Basom, R., Delrow, J.J., Overbaugh, J., and Emerman, M. (2018). A virus-packageable CRISPR screen identifies host factors mediating interferon inhibition of HIV. Elife *7*. 10.7554/eLife.39823.

19. Siddiqui, M.A., Saito, A., Halambage, U.D., Ferhadian, D., Fischer, D.K., Francis, A.C., Melikyan, G.B., Ambrose, Z., Aiken, C., and Yamashita, M. (2019). A Novel Phenotype Links HIV-1 Capsid Stability to cGAS-Mediated DNA Sensing. J Virol *93*. 10.1128/JVI.00706-19.

20. Papa, G., Albecka, A., Mallery, D., Vaysburd, M., Renner, N., and James, L.C. (2023). IP6-stabilised HIV capsids evade cGAS/STING-mediated host immune sensing. EMBO reports *24*, e56275. 10.15252/embr.202256275.

21. Zuliani-Alvarez, L., Govasli, M.L., Rasaiyaah, J., Monit, C., Perry, S.O., Sumner, R.P., McAlpine-Scott, S., Dickson, C., Rifat Faysal, K.M., Hilditch, L., et al. (2022). Evasion of cGAS and TRIM5 defines pandemic HIV. Nat Microbiol *7*, 1762–1776. 10.1038/s41564-022-01247-0.

22. Lahaye, X., Gentili, M., Silvin, A., Conrad, C., Picard, L., Jouve, M., Zueva, E., Maurin, M., Nadalin, F., Knott, G.J., et al. (2018). NONO Detects the Nuclear HIV Capsid to Promote cGAS-Mediated Innate Immune Activation. Cell *175*, 488-501 e22. 10.1016/j.cell.2018.08.062.

23. Yoh, S.M., Mamede, J.I., Lau, D., Ahn, N., Sánchez-Aparicio, M.T., Temple, J., Tuckwell, A., Fuchs, N.V., Cianci, G.C., Riva, L., et al. (2022). Recognition of HIV-1 capsid by PQBP1

licenses an innate immune sensing of nascent HIV-1 DNA. Mol Cell *82*, 2871-2884.e6. 10.1016/j.molcel.2022.06.010.

24. Eschbach, J.E., Puray-Chavez, M., Mohammed, S., Wang, Q., Xia, M., Huang, L.-C., Shan, L., and Kutluay, S.B. (2024). HIV-1 capsid stability and reverse transcription are finely balanced to minimize sensing of reverse transcription products via the cGAS-STING pathway. mBio *0*, e00348-24. 10.1128/mbio.00348-24.

25. Dick, R.A., Zadrozny, K.K., Xu, C., Schur, F.K.M., Lyddon, T.D., Ricana, C.L., Wagner, J.M., Perilla, J.R., Ganser-Pornillos, B.K., Johnson, M.C., et al. (2018). Inositol phosphates are assembly co-factors for HIV-1. Nature *560*, 509–512. 10.1038/s41586-018-0396-4.

26. Mallery, D.L., Márquez, C.L., McEwan, W.A., Dickson, C.F., Jacques, D.A., Anandapadamanaban, M., Bichel, K., Towers, G.J., Saiardi, A., Böcking, T., et al. (2018). IP6 is an HIV pocket factor that prevents capsid collapse and promotes DNA synthesis. Elife *7*, e35335. 10.7554/eLife.35335.

27. Jennings, J., Shi, J., Varadarajan, J., Jamieson, P.J., and Aiken, C. (2020). The Host Cell Metabolite Inositol Hexakisphosphate Promotes Efficient Endogenous HIV-1 Reverse Transcription by Stabilizing the Viral Capsid. mBio *11*, 10.1128/mbio.02820-20. 10.1128/mbio.02820-20.

28. Forshey, B.M., von Schwedler, U., Sundquist, W.I., and Aiken, C. (2002). Formation of a human immunodeficiency virus type 1 core of optimal stability is crucial for viral replication. J Virol *76*, 5667–5677. 10.1128/jvi.76.11.5667-5677.2002.

29. von Schwedler, U.K., Stray, K.M., Garrus, J.E., and Sundquist, W.I. (2003). Functional Surfaces of the Human Immunodeficiency Virus Type 1 Capsid Protein. Journal of Virology *77*, 5439–5450. 10.1128/jvi.77.9.5439-5450.2003.

30. Ganser-Pornillos, B.K., von Schwedler, U.K., Stray, K.M., Aiken, C., and Sundquist, W.I. (2004). Assembly Properties of the Human Immunodeficiency Virus Type 1 CA Protein. Journal of Virology *78*, 2545–2552. 10.1128/jvi.78.5.2545-2552.2004.

31. Sowd, G.A., Shi, J., Fulmer, A., and Aiken, C. (2023). HIV-1 capsid stability enables inositol phosphate-independent infection of target cells and promotes integration into genes. PLOS Pathogens *19*, e1011423. 10.1371/journal.ppat.1011423.

32. Kleinpeter, A.B., Zhu, Y., Mallery, D.L., Ablan, S.D., Chen, L., Hardenbrook, N., Saiardi, A., James, L.C., Zhang, P., and Freed, E.O. (2023). The Effect of Inositol Hexakisphosphate on HIV-1 Particle Production and Infectivity can be Modulated by Mutations that Affect the Stability of the Immature Gag Lattice. Journal of Molecular Biology *435*, 168037. 10.1016/j.jmb.2023.168037.

33. Letcher, A.J., Schell, M.J., and Irvine, R.F. (2008). Do mammals make all their own inositol hexakisphosphate? Biochem J *416*, 263–270. 10.1042/BJ20081417.

34. Kumar, S., Morrison, J.H., Dingli, D., and Poeschla, E. (2018). HIV-1 Activation of Innate Immunity Depends Strongly on the Intracellular Level of TREX1 and Sensing of Incomplete Reverse Transcription Products. J Virol *92*. 10.1128/JVI.00001-18.

35. Yant, S.R., Mulato, A., Hansen, D., Tse, W.C., Niedziela-Majka, A., Zhang, J.R., Stepan, G.J., Jin, D., Wong, M.H., Perreira, J.M., et al. (2019). A highly potent long-acting small-molecule HIV-1 capsid inhibitor with efficacy in a humanized mouse model. Nat Med *25*, 1377–1384. 10.1038/s41591-019-0560-x.

36. Link, J.O., Rhee, M.S., Tse, W.C., Zheng, J., Somoza, J.R., Rowe, W., Begley, R., Chiu, A., Mulato, A., Hansen, D., et al. (2020). Clinical targeting of HIV capsid protein with a long-acting small molecule. Nature *584*, 614–618. 10.1038/s41586-020-2443-1.

37. Faysal, K.R., Walsh, J.C., Renner, N., Márquez, C.L., Shah, V.B., Tuckwell, A.J., Christie, M.P., Parker, M.W., Turville, S.G., Towers, G.J., et al. (2024). Pharmacologic hyperstabilisation of the HIV-1 capsid lattice induces capsid failure. eLife *13*, e83605. 10.7554/eLife.83605.

38. Blair, W.S., Pickford, C., Irving, S.L., Brown, D.G., Anderson, M., Bazin, R., Cao, J., Ciaramella, G., Isaacson, J., Jackson, L., et al. (2010). HIV Capsid is a Tractable Target for Small Molecule Therapeutic Intervention. PLoS Pathog *6*, e1001220. 10.1371/journal.ppat.1001220.

39. Bhattacharya, A., Alam, S.L., Fricke, T., Zadrozny, K., Sedzicki, J., Taylor, A.B., Demeler, B., Pornillos, O., Ganser-Pornillos, B.K., Diaz-Griffero, F., et al. (2014). Structural basis of HIV-1 capsid recognition by PF74 and CPSF6. Proceedings of the National Academy of Sciences *111*, 18625–18630. 10.1073/pnas.1419945112.

40. Segal-Maurer, S., DeJesus, E., Stellbrink, H.-J., Castagna, A., Richmond, G.J., Sinclair, G.I., Siripassorn, K., Ruane, P.J., Berhe, M., Wang, H., et al. (2022). Capsid Inhibition with Lenacapavir in Multidrug-Resistant HIV-1 Infection. N Engl J Med *386*, 1793–1803. 10.1056/NEJMoa2115542.

41. Bester, S.M., Wei, G., Zhao, H., Adu-Ampratwum, D., Iqbal, N., Courouble, V.V., Francis, A.C., Annamalai, A.S., Singh, P.K., Shkriabai, N., et al. (2020). Structural and mechanistic bases for a potent HIV-1 capsid inhibitor. Science *370*, 360–364. 10.1126/science.abb4808.

42. Schirra, R.T., dos Santos, N.F.B., Zadrozny, K.K., Kucharska, I., Ganser-Pornillos, B.K., and Pornillos, O. (2023). A molecular switch modulates assembly and host factor binding of the HIV-1 capsid. Nat Struct Mol Biol *30*, 383–390. 10.1038/s41594-022-00913-5.

43. Sanjana, N.E., Shalem, O., and Zhang, F. (2014). Improved vectors and genome-wide libraries for CRISPR screening. Nat Methods *11*, 783–784. 10.1038/nmeth.3047.

44. Yoh, S.M., Schneider, M., Seifried, J., Soonthornvacharin, S., Akleh, R.E., Olivieri, K.C., De Jesus, P.D., Ruan, C., de Castro, E., Ruiz, P.A., et al. (2015). PQBP1 Is a Proximal Sensor of the cGAS-Dependent Innate Response to HIV-1. Cell *161*, 1293–1305. 10.1016/j.cell.2015.04.050.

45. Hrecka, K., Hao, C., Gierszewska, M., Swanson, S.K., Kesik-Brodacka, M., Srivastava, S., Florens, L., Washburn, M.P., and Skowronski, J. (2011). Vpx relieves inhibition of HIV-1 infection of macrophages mediated by the SAMHD1 protein. Nature *474*, 658–661. 10.1038/nature10195.

46. Laguette, N., Sobhian, B., Casartelli, N., Ringeard, M., Chable-Bessia, C., Segeral, E., Yatim, A., Emiliani, S., Schwartz, O., and Benkirane, M. (2011). SAMHD1 is the dendritic- and myeloid-cell-specific HIV-1 restriction factor counteracted by Vpx. Nature *474*, 654–657. 10.1038/nature10117.

47. McCauley, S.M., Kim, K., Nowosielska, A., Dauphin, A., Yurkovetskiy, L., Diehl, W.E., and Luban, J. (2018). Intron-containing RNA from the HIV-1 provirus activates type I interferon and inflammatory cytokines. Nat Commun *9*, 5305. 10.1038/s41467-018-07753-2.

48. Akiyama, H., Miller, C.M., Ettinger, C.R., Belkina, A.C., Snyder-Cappione, J.E., and Gummuluru, S. (2018). HIV-1 intron-containing RNA expression induces innate immune activation and T cell dysfunction. Nat Commun *9*, 3450. 10.1038/s41467-018-05899-7.

49. Gondim, M.V.P., Sherrill-Mix, S., Bibollet-Ruche, F., Russell, R.M., Trimboli, S., Smith, A.G., Li, Y., Liu, W., Avitto, A.N., DeVoto, J.C., et al. (2021). Heightened resistance to host type 1 interferons characterizes HIV-1 at transmission and after antiretroviral therapy interruption. Sci Transl Med *13*. 10.1126/scitranslmed.abd8179.

50. Iyer, S.S., Bibollet-Ruche, F., Sherrill-Mix, S., Learn, G.H., Plenderleith, L., Smith, A.G., Barbian, H.J., Russell, R.M., Gondim, M.V., Bahari, C.Y., et al. (2017). Resistance to type 1 interferons is a major determinant of HIV-1 transmission fitness. Proc Natl Acad Sci U S A *114*, E590–E599. 10.1073/pnas.1620144114.

51. Beignon, A.S., McKenna, K., Skoberne, M., Manches, O., DaSilva, I., Kavanagh, D.G., Larsson, M., Gorelick, R.J., Lifson, J.D., and Bhardwaj, N. (2005). Endocytosis of HIV-1 activates plasmacytoid dendritic cells via Toll-like receptor-viral RNA interactions. The Journal of clinical investigation *115*, 3265–3275. 10.1172/JCI26032.

52. Lepelley, A., Louis, S., Sourisseau, M., Law, H.K., Pothlichet, J., Schilte, C., Chaperot, L., Plumas, J., Randall, R.E., Si-Tahar, M., et al. (2011). Innate sensing of HIV-infected cells. PLoS Pathog *7*, e1001284. 10.1371/journal.ppat.1001284.

53. Wang, Q., Gao, H., Clark, K.M., Mugisha, C.S., Davis, K., Tang, J.P., Harlan, G.H., DeSelm, C.J., Presti, R.M., Kutluay, S.B., et al. (2021). CARD8 is an inflammasome sensor for HIV-1 protease activity. Science *371*. 10.1126/science.abe1707.

54. Monroe, K.M., Yang, Z., Johnson, J.R., Geng, X., Doitsh, G., Krogan, N.J., and Greene, W.C. (2014). IFI16 DNA sensor is required for death of lymphoid CD4 T cells abortively infected with HIV. Science *343*, 428–432. 10.1126/science.1243640.

55. Doitsh, G., Cavrois, M., Lassen, K.G., Zepeda, O., Yang, Z., Santiago, M.L., Hebbeler, A.M., and Greene, W.C. (2010). Abortive HIV Infection Mediates CD4 T-Cell Depletion and Inflammation in Human Lymphoid Tissue. Cell *143*, 789–801. 10.1016/j.cell.2010.11.001.

56. Martin-Gayo, E., Buzon, M.J., Ouyang, Z., Hickman, T., Cronin, J., Pimenova, D., Walker, B.D., Lichterfeld, M., and Yu, X.G. (2015). Potent Cell-Intrinsic Immune Responses in Dendritic Cells Facilitate HIV-1-Specific T Cell Immunity in HIV-1 Elite Controllers. PLoS Pathog *11*, e1004930. 10.1371/journal.ppat.1004930.

57. Martin-Gayo, E., Cole, M.B., Kolb, K.E., Ouyang, Z., Cronin, J., Kazer, S.W., Ordovas-Montanes, J., Lichterfeld, M., Walker, B.D., Yosef, N., et al. (2018). A Reproducibility-Based

Computational Framework Identifies an Inducible, Enhanced Antiviral State in Dendritic Cells from HIV-1 Elite Controllers. Genome Biol *19*, 10. 10.1186/s13059-017-1385-x.

58. Migueles, S.A., Laborico, A.C., Shupert, W.L., Sabbaghian, M.S., Rabin, R., Hallahan, C.W., Van Baarle, D., Kostense, S., Miedema, F., McLaughlin, M., et al. (2002). HIV-specific CD8+ T cell proliferation is coupled to perforin expression and is maintained in nonprogressors. Nat Immunol *3*, 1061–1068. 10.1038/ni845.

59. Ndhlovu, Z.M., Kamya, P., Mewalal, N., Kloverpris, H.N., Nkosi, T., Pretorius, K., Laher, F., Ogunshola, F., Chopera, D., Shekhar, K., et al. (2015). Magnitude and Kinetics of CD8+ T Cell Activation during Hyperacute HIV Infection Impact Viral Set Point. Immunity *43*, 591–604. 10.1016/j.immuni.2015.08.012.

60. Jeremiah, N., Ferran, H., Antoniadou, K., De Azevedo, K., Nikolic, J., Maurin, M., Benaroch, P., and Manel, N. (2023). RELA tunes innate-like interferon I/III responses in human T cells. J Exp Med *220*, e20220666. 10.1084/jem.20220666.

61. Elsner, C., Ponnurangam, A., Kazmierski, J., Zillinger, T., Jansen, J., Todt, D., Dohner, K., Xu, S., Ducroux, A., Kriedemann, N., et al. (2020). Absence of cGAS-mediated type I IFN responses in HIV-1-infected T cells. Proc Natl Acad Sci U S A *117*, 19475–19486. 10.1073/pnas.2002481117.

62. Greiner, D., Scott, T.M., Olson, G.S., Aderem, A., Roh-Johnson, M., and Johnson, J.S. (2022). Genetic Modification of Primary Human Myeloid Cells to Study Cell Migration, Activation, and Organelle Dynamics. Curr Protoc *2*, e514. 10.1002/cpz1.514.

63. Mangeot, P.E., Nègre, D., Dubois, B., Winter, A.J., Leissner, P., Mehtali, M., Kaiserlian, D., Cosset, F.L., and Darlix, J.L. (2000). Development of minimal lentivirus vectors derived from simian immunodeficiency virus (SIVmac251) and their use for gene transfer into human dendritic cells. J. Virol. *74*, 8307–8315.

64. Ott, D.E. (2009). Purification of HIV-1 Virions by Subtilisin Digestion or CD45 Immunoaffinity Depletion for Biochemical Studies. In HIV Protocols Methods In Molecular Biology™., V. R. Prasad and G. V. Kalpana, eds. (Humana Press), pp. 15–25. 10.1007/978-1-59745-170-3_2.

65. Zhou, W., Whiteley, A.T., de Oliveira Mann, C.C., Morehouse, B.R., Nowak, R.P., Fischer, E.S., Gray, N.S., Mekalanos, J.J., and Kranzusch, P.J. (2018). Structure of the Human cGAS–DNA Complex Reveals Enhanced Control of Immune Surveillance. Cell *174*, 300-311.e11. 10.1016/j.cell.2018.06.026.

66. Zhou, W., Whiteley, A.T., and Kranzusch, P.J. (2019). Chapter Two - Analysis of human cGAS activity and structure. In Methods in Enzymology DNA Sensors and Inflammasomes., J. Sohn, ed. (Academic Press), pp. 13–40. 10.1016/bs.mie.2019.04.012.

67. Kennedy, E.M., Gavegnano, C., Nguyen, L., Slater, R., Lucas, A., Fromentin, E., Schinazi, R.F., and Kim, B. (2010). Ribonucleoside triphosphates as substrate of human immunodeficiency virus type 1 reverse transcriptase in human macrophages. J Biol Chem *285*, 39380–39391. 10.1074/jbc.M110.178582.

68. Diamond, T.L., Roshal, M., Jamburuthugoda, V.K., Reynolds, H.M., Merriam, A.R., Lee, K.Y., Balakrishnan, M., Bambara, R.A., Planelles, V., Dewhurst, S., et al. (2004). Macrophage tropism of HIV-1 depends on efficient cellular dNTP utilization by reverse transcriptase. J Biol Chem *279*, 51545–51553. 10.1074/jbc.M408573200.

69. Wang, C., Guan, Y., Lv, M., Zhang, R., Guo, Z., Wei, X., Du, X., Yang, J., Li, T., Wan, Y., et al. (2018). Manganese Increases the Sensitivity of the cGAS-STING Pathway for Double-Stranded DNA and Is Required for the Host Defense against DNA Viruses. Immunity *48*, 675-687 e7. 10.1016/j.immuni.2018.03.017.

Figures and Legends

Figure 1.

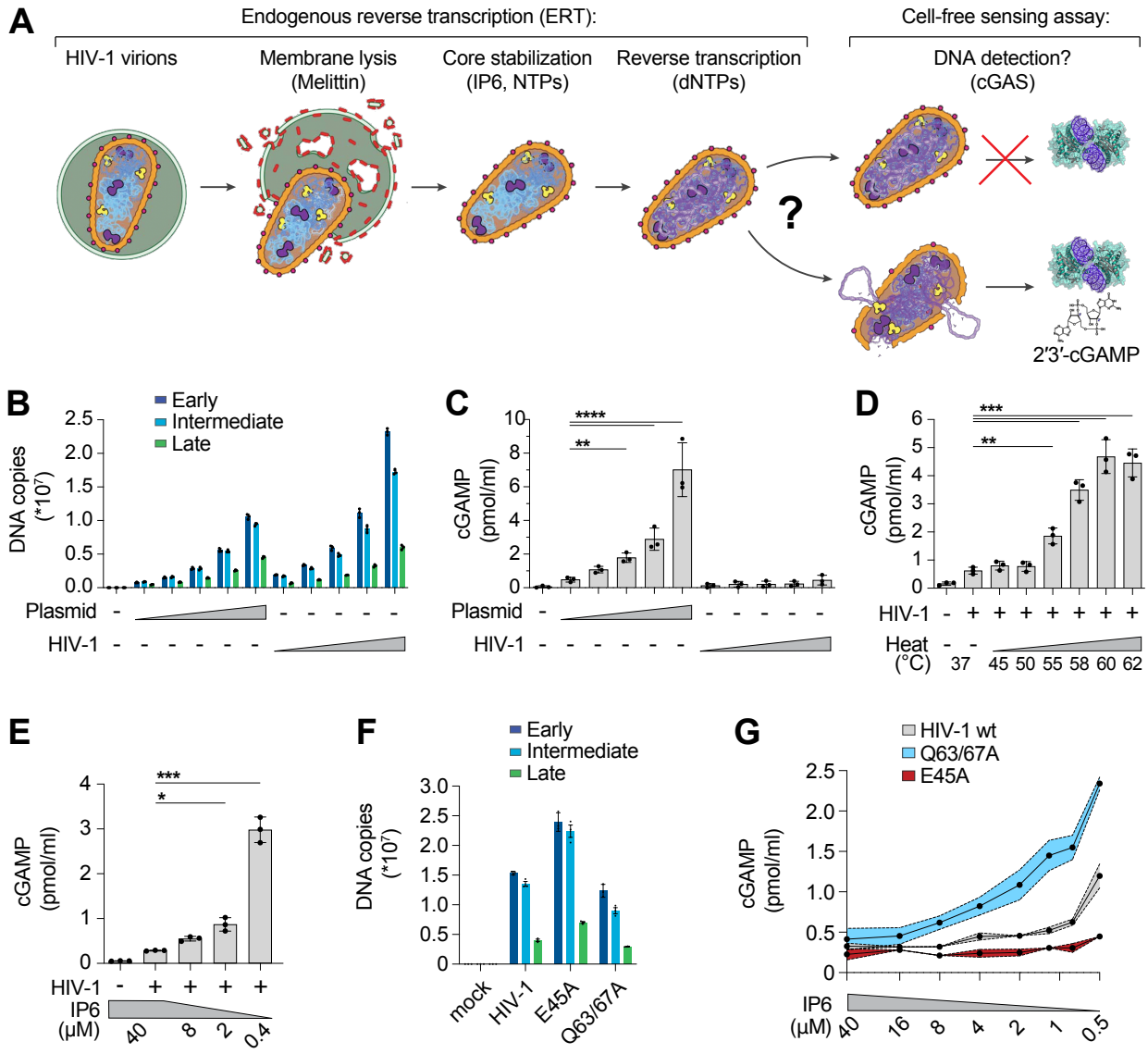

Figure 1. The HIV-1 capsid protects RT products from cGAS in vitro.

(A) Steps in the endogenous reverse transcription (ERT) and cell-free sensing assays. Capsids that remain intact after ERT may protect viral DNA from detection and capsids that lose integrity may permit cGAS activation and cGAMP production.

(B) qPCR measurements of plasmid DNA control containing the viral genome sequence compared to HIV-1 ERT reactions in 2-fold dilution series, incubated for 16 h under identical conditions. Primer sets detect sequences for early (minus strand strong stop), intermediate (first strand transfer), and late RT (second strand transfer), which are present in both the plasmid and viral genome.

(C) Cell-free sensing assay for samples shown in (B) incubated with recombinant cGAS. cGAMP levels were determined by ELISA (applies to all cell-free sensing assays).

(D) Cell-free sensing assay of heat treated ERT samples. Samples were held at the indicated temperatures (20 s) and then subject to cell-free sensing assays performed under standard conditions.

(E) Cell-free sensing assay of ERT samples incubated with cGAS under a range of IP6 concentrations.

(F) qPCR measurements of DNA copy numbers from ERT reactions with wt HIV-1 virions compared to virions with stabilizing (E45A) or destabilizing (Q63/67A) mutations in CA.

(G) Cell-free sensing assay of wt, E45A, or Q63/67A ERT samples after normalizing for DNA input and incubating with cGAS at the indicated IP6 concentrations. Statistics were calculated using a one-way ANOVA with Tukey's multiple comparisons test: $p<0.05$: *, $p<0.01$: **, $p<0.001$: ***, $p<0.0001$: ****. Graphs depict mean ± SD from three samples from a representative experiment, selected from three independent experiments.

Figure 2.

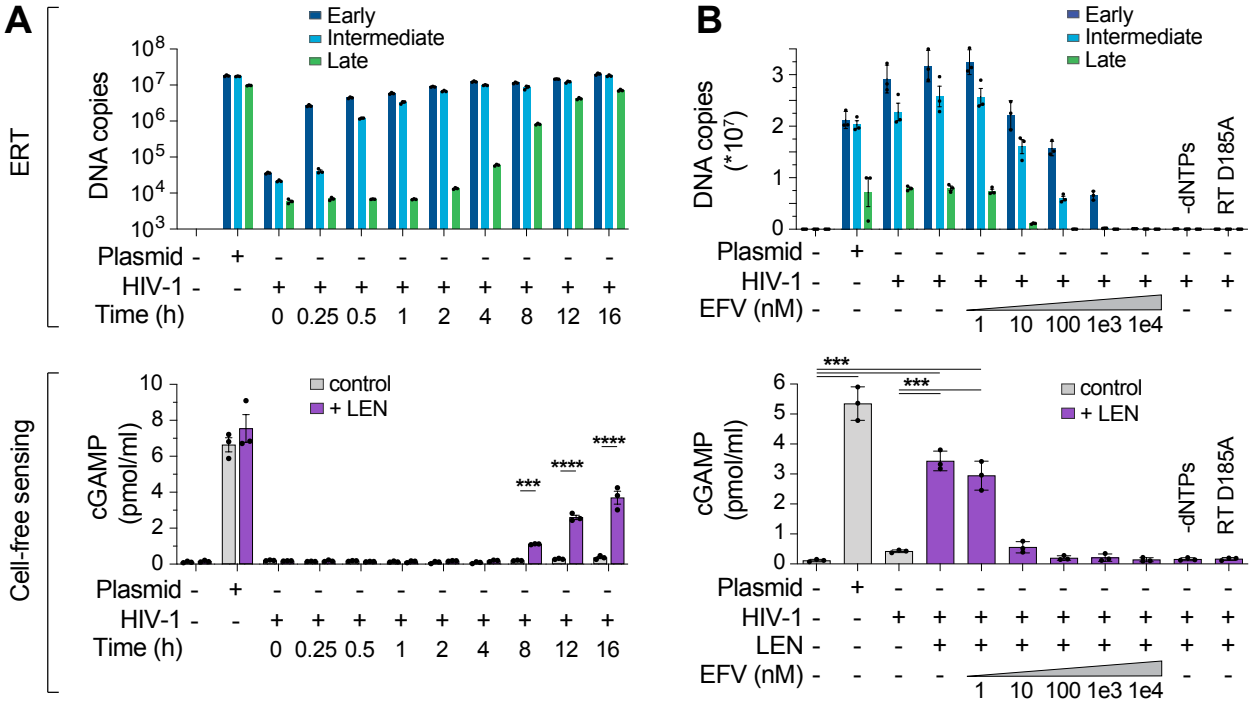
A
ERT
Early
Intermediate
Late
DNA copies
Plasmid
HIV-1
Time (h)
0 0.25 0.5 1 2 4 8 12 16
Cell-free sensing
control
+ LEN
cGAMP (pmol/ml)
***
****
B
DNA copies (*10^7)
-dNTPs
RT D185A
EFV (nM)
1 10 100 1e3 1e4
LEN

Figure 2. Lenacapavir triggers cGAS sensing of HIV-1 reverse transcripts.

(A) DNA product levels from an HIV-1 ERT time course compared to a plasmid control, as measured by qPCR (top panel), and cell-free sensing assays for the same samples incubated with recombinant cGAS ±LEN (100 nM) (bottom panel).

(B) DNA products (top panel) and cell-free cGAS activity (bottom panel) for ERT reactions performed in the presence of increasing concentrations of the RT inhibitor efavirenz (EFV), or without dNTPs, or using a virus containing an inactivating mutation in RT (D185A). Statistics were calculated using a one-way ANOVA with Tukey's multiple comparisons test: $p<0.001$: ***, $p<0.0001$: ****. Graphs depict mean ± SD from three samples from a representative experiment, selected from three independent experiments.

Figure 3.

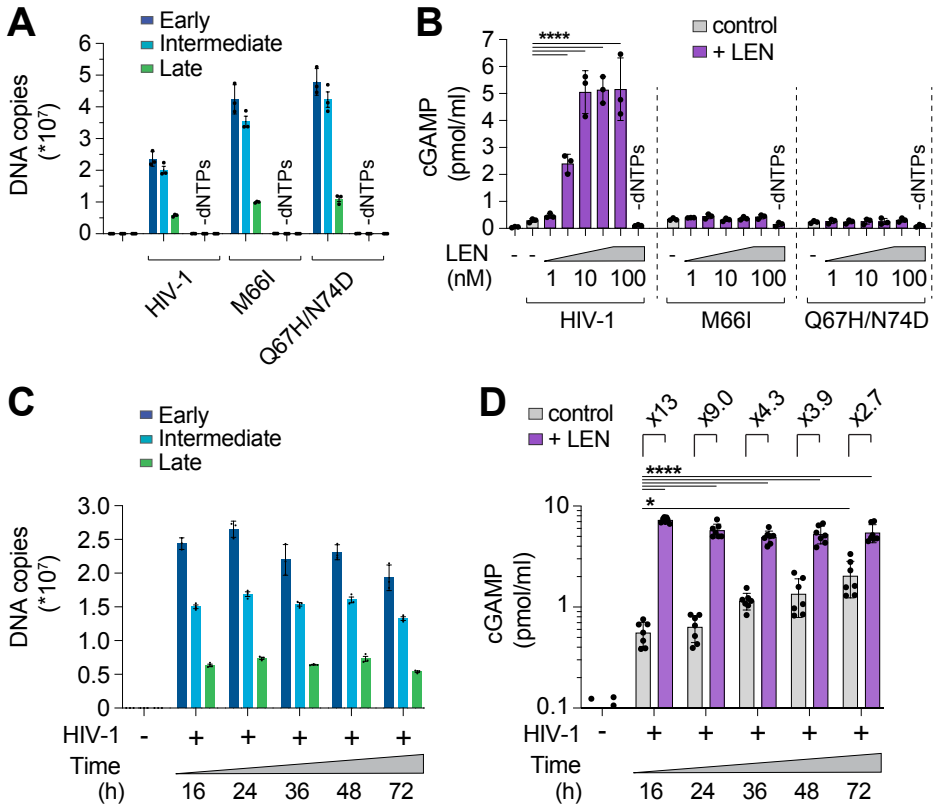
A
Early
Intermediate
Late
DNA copies (*10^7)
-dNTPs
HIV-1
M66I
Q67H/N74D
B
control
+ LEN
****
cGAMP (pmol/ml)
LEN (nM)
1 10 100
C
Time (h)
16 24 36 48 72
D
x13
x9.0
x4.3
x3.9
x2.7
*

Figure 3. CA mutations confer resistance to LEN-triggered cGAS activation.

(A) qPCR measurements of DNA copy number from ERT reactions with wt HIV-1 virions compared to virions bearing LEN resistance-associated mutations in CA (M66I and Q67H/N74D), performed with or without dNTPs.

(B) Cell-free sensing assay of wt, M66I, or Q67H/N74D ERT samples that were incubated with increasing amounts of LEN (0, 1, 3.2, 10, 32, 100 nM), or LEN (100 nM) −dNTPs.

(C) qPCR measurements of DNA copy number for ERT reactions held at 37°C for the indicated times.

(D) Cell-free sensing assay of ERT samples from (C) after normalizing for late RT DNA copy number and reacting with recombinant cGAS (±LEN at 100 nM).

Statistics were calculated using a one-way ANOVA with Tukey's multiple comparisons test: $p<0.05$: *, $p<0.0001$: ****. Graphs depict mean ± SD from three measurements from a representative experiment, selected from 3 independent experiments (A–C) or from 7 independent samples measured on different days (D).

Figure 4.

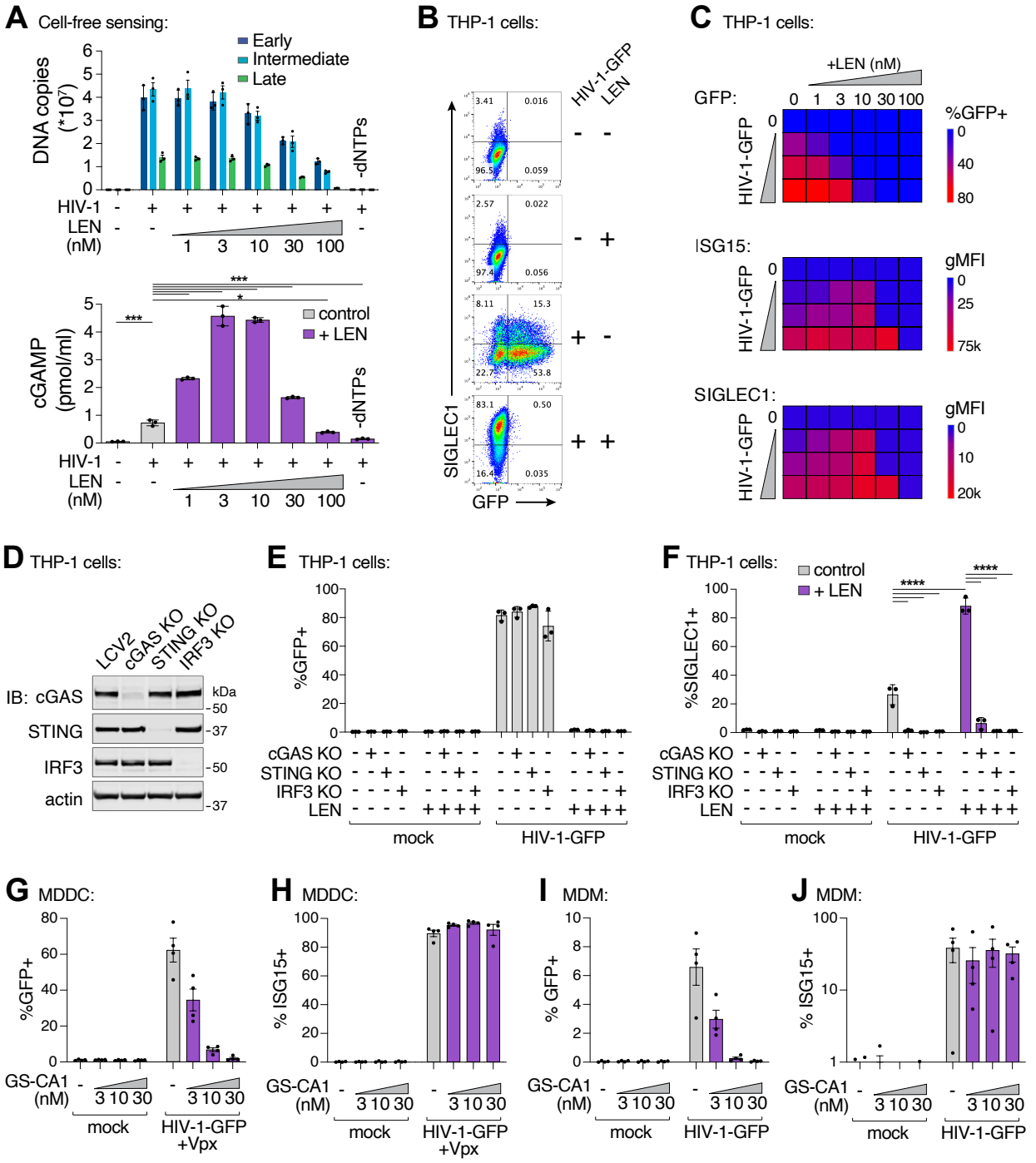
A Cell-free sensing:
Early
Intermediate
Late
DNA copies (*10^7)
-dNTPs
HIV-1
LEN (nM)
1 3 10 30 100
cGAMP (pmol/ml)
control
+ LEN
B THP-1 cells:
HIV-1-GFP
LEN
SIGLEC1
GFP
C THP-1 cells:
+LEN (nM)
GFP:
0 1 3 10 30 100
HIV-1-GFP
%GFP+
ISG15:
gMFI
SIGLEC1:
D THP-1 cells:
LCV2
cGAS KO
STING KO
IRF3 KO
IB: cGAS
STING
IRF3
actin
kDa
E THP-1 cells:
%GFP+
cGAS KO
STING KO
IRF3 KO
LEN
mock
HIV-1-GFP
F THP-1 cells:
control
+ LEN
%SIGLEC1+
G MDDC:
%GFP+
GS-CA1 (nM)
3 10 30
mock
HIV-1-GFP +Vpx
H MDDC:
% ISG15+
I MDM:
% GFP+
J MDM:
% ISG15+

Figure 4. Capsid inhibitors potentiate sensing of HIV-1 through the cGAS-STING pathway in cells.

(A) qPCR measurements of DNA copy number from ERT reactions with the indicated concentrations of LEN (top panel) and cell-free sensing assays (bottom panel) performed with the same samples and the same concentrations of LEN.

(B) Flow cytometry of THP-1 monocytic cells infected with HIV-1-GFP for 48 h (±LEN at 10 nM), showing expression of GFP (viral infectivity) and SIGLEC1 (IFN response).

(C) Heat maps of GFP, ISG15, and SIGLEC1 expression as determined by flow cytometry of THP-1 cells infected with HIV-1-GFP for 48 h. Columns show a range of LEN concentrations and rows show increasing virus doses (12.5, 25, and 50 nM p24). n = 3.

(D) Immunoblots of THP-1 lysates after lentiCRISPR editing, depicting knockout of cGAS, STING, or IRF3 relative to a non-targeting vector control (LCV2).

(E–F) Flow cytometry of lentiCRISPR-modified THP-1 cells infected with HIV-1-GFP (25 nM p24) for 48 h, showing the percent of cells positive for GFP (E) or SIGLEC1 (F) expression for the indicated conditions (±LEN at 10 nM).

(G–H) Flow cytometry of MDDCs derived from 4 separate donors that were infected with HIV-1-GFP for 48 h with increasing concentrations of GS-CA1. Vpx was included to overcome SAMHD1-mediated restriction. Panels show infectivity (GFP+, G) and IFN induction (ISG15+, H).

(I–J) Flow cytometry of MDMs from 4 donors that were infected with HIV-1-GFP in the same fashion as in (G–H) without Vpx. Graphs depict the percentage of GFP (G,I) or ISG15 (H,J) positive cells. For (A,F), statistics were calculated using a one-way ANOVA with Tukey's multiple comparisons test: $p<0.05$: *, $p<0.001$: ***, $p<0.0001$: ****. Graphs depict mean ± SD from three samples from a representative experiment, selected from 2–3 independent experiments, unless otherwise noted.